JCTC Journal of Chemical Theory and Computation

Article

pubs.acs.org/JCTC

Performance of DFT Methods in Momentum Space: Quantum Similarity Measures versus Moments of Momentum

Jelle Vandenbussche,* Guillaume Acke, and Patrick Bultinck*

Department of Inorganic and Physical Chemistry, Ghent University, Krijgslaan 281 (S3), 9000 Ghent, Belgium

Supporting Information

ABSTRACT: The quality of momentum space electron densities obtained from a large array of density functionals is investigated through careful numerical comparison with the density obtained using reference CCSD calculations. Using a test set of 68 closed-shell molecules in their ground state and 77 different computational methods, including coupled cluster, MP2 perturbation theory, Hartree−Fock, and a total of 74 DFT functionals, including long-range corrected functionals, we confirm that DFT momentum densities generally show poorer agreement with the reference than MP2 densities. The performance of DFT functionals varies significantly with only 8 DFT functionals outperforming Hartree−Fock with respect to electron momentum densities and their spherically averaged counterparts.

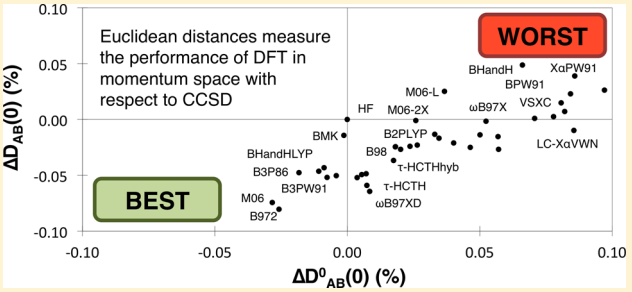

INTRODUCTION

Quantum mechanics has no preference for the basis in which the wave function is expressed, and as a consequence one can equivalently opt for either a position representation or a momentum representation.[1] Although both are equivalent, there is a clear bias toward the position representation, especially among chemists. The reason is the familiarity of the majority of chemists with concepts deeply rooted in a (Born−Oppenheimer) context of conformations, chirality, regioselectivity, etc. This leads to the fact that, however numerous momentum space based quantum chemical work, the number of such studies perishes in front of the number of papers that rely on the position representation. The degree of awareness of the equivalence of both position and momentum spaces and the consequent requirement of computational methods to perform well in both of them still needs to grow among many chemists.

Of prime interest in quantum chemistry are the electron density and density matrices, again mostly expressed in position space. The **p**-space counterpart of the **r**-space electron charge density $\rho(\boldsymbol{r})$ is the electron momentum density $\Pi(\boldsymbol{p})$, obtained from the momentum space wave function $\Phi(\boldsymbol{y}_1,\boldsymbol{y}_2,\ldots,\boldsymbol{y}_N)$ through[2]

$$\Pi(\boldsymbol{p}) = N\int |\Phi(\boldsymbol{y}_1, \boldsymbol{y}_2, \ldots, \boldsymbol{y}_N)|^2 \delta(\boldsymbol{p} - \boldsymbol{p}_1) d\boldsymbol{y}_1 d\boldsymbol{y}_2 \ldots d\boldsymbol{y}_N \quad (1)$$

where $\boldsymbol{y}_k$ represents the momentum-spin coordinates $(\boldsymbol{p}_k,\boldsymbol{\omega}_k)$ of electron k, and N is the number of electrons.

There are several ways to obtain the momentum space wave function $\Phi(\boldsymbol{y}_1,\boldsymbol{y}_2,\ldots,\boldsymbol{y}_N)$. The most common approach is to first compute the position space wave function $\Psi(\boldsymbol{x}_1,\boldsymbol{x}_2,\ldots,\boldsymbol{x}_N)$ (with $\boldsymbol{x}_k = (\boldsymbol{r}_k,\boldsymbol{\omega}_k)$, the position-spin coordinates) and then Fourier transform it,[1] although the direct solution of quantum chemical equations, such as the Hartree−Fock (HF) equations in momentum space, has also become tractable.[3] This study uses the most common and indirect, Fourier transform, route given by[2]

$$\Phi(\boldsymbol{y}_1, \boldsymbol{y}_2, \ldots, \boldsymbol{y}_N) = (2\pi)^{-3N/2} \int \Psi(\boldsymbol{x}_1, \boldsymbol{x}_2, \ldots, \boldsymbol{x}_N) e^{-i[\sum_{k=1}^{N} \boldsymbol{p}_k \cdot \boldsymbol{r}_k]} d\boldsymbol{r}_1 d\boldsymbol{r}_2 \ldots d\boldsymbol{r}_N \quad (2)$$

Whereas for many chemists, $\rho(\boldsymbol{r})$ and related quantities offer immediate insight, for instance for the regioselectivity of chemical reactions, $\Pi(\boldsymbol{p})$ reveals different information in an often less intuitive way. First and most important, this is due to the fact that $\Pi(\boldsymbol{p})$ is a monocentric distribution. The lack of a nuclear centered framework requires a totally different chain of thought to approach/recognize molecules. Second, the microreversibility principle is met through the presence of an inversion center:[4]

$$\Pi(\boldsymbol{p}) = \Pi(-\boldsymbol{p}) \quad (3)$$

Consequently $\Pi(\boldsymbol{p})$ is a highly symmetric distribution. Due to this 'collapsed' character,[5] the only remaining meaningful position related feature is the sense of direction which is preserved throughout the Fourier transformation in eq 2. Nonetheless, $\Pi(\boldsymbol{p})$ shows significant chemically interesting features, even beyond Compton Scattering experiments where $\Pi(\boldsymbol{p})$ plays the key role.[6] This is attested, among others, through momentum space quantum similarity studies.[7]

Received: April 2, 2013

dx.doi.org/10.1021/ct400266g | J. Chem. Theory Comput. XXXX, XXX, XXX−XXX

The performance of different quantum chemical methods is often assessed in terms of their agreement with experiment or in terms of the agreement between expectation values obtained with some computational technique compared to those obtained with a high level method. Some landmark papers studying the performance of ab initio techniques in momentum space have appeared. These studies by e.g. Hart and Thakkar[8] and Miquel and de la Vega[9] mainly relied on the comparison of moments of momentum between ab initio methods with some advanced level of theory as reference. Alternatively, in what is known as quantum similarity,[10] the electron densities are compared directly. The aim of the present study is to examine the performance of DFT methods for generating momentum space electron densities through direct comparison between the densities themselves with respect to the density obtained using a high level ab initio method. To that end, the set of functionals considered is extended from the few used in the previous works to a set containing functionals of all types used nowadays such that a more general conclusion can be drawn on the DFT performance.

The paper is organized as follows. First an overview of previous work is presented together with the present methodology, followed by the results and their discussion.

METHODOLOGY

We first discuss briefly the previously used approaches[8,9,11] for describing the performance of quantum chemical methods in momentum space, with emphasis on the work by Hart and Thakkar[8] and the work by Miguel and de la Vega.[9]

The topological features of $\Pi(\boldsymbol{p})$ generated using different ab initio methods and/or basis sets for one and the same molecule have been investigated in relatively few studies.[11a−c] This has proven quite intricate, the main reasons for which are the complexity of comparing three-dimensional monocentric distributions with subtle features and the wide plethora of computational methods that is currently available. Consequently, comparisons are more commonly based on the spherically averaged electron momentum distribution $\Pi^0(\boldsymbol{p})$, the radial momentum distribution,[9] or the isotropic Compton profile,[11d] which are easy to visualize but where a large part of the original anisotropy of $\Pi(\boldsymbol{p})$ is lost.

The original anisotropy of $\Pi(\boldsymbol{p})$ is reflected in Compton profile anisotropies. In contrast to gas phase Compton Scattering[12] experiments which only allow the measurement of the isotropic Compton profile, solid-state experiments additionally allow the determination of directional Compton profiles. By taking the difference of directional Compton profiles, the Compton profile anisotropy can be obtained both experimentally and computationally.[2,5,13] Through cylindrical averaging, weak features in $\Pi(\boldsymbol{p})$ for large systems may become even weaker in the Compton profile anisotropy.

A yet more common way to assess the performance of a method in **p**-space is by comparing its moments of momentum with respect to a reference (high level of theory or experiment).[8,9,11d] The moments of the electronic momentum density measure the amount of momentum density in different **p**-space regions and are defined as

$$\langle p^k \rangle = \int p^k \Pi(\boldsymbol{p}) d\boldsymbol{p} = 4\pi \int_0^\infty p^{k+2} \Pi^0(p) dp \tag{4}$$

with k ranging from −2 to 4.[2] The performance of a method A is evaluated by calculating the absolute percentage error in moment with respect to a reference distribution B as[8]

$$\%E_k = 100 \cdot \frac{|\langle p^k \rangle_A - \langle p^k \rangle_B|}{\langle p^k \rangle_B} = 100 \cdot \frac{N}{\langle p^k \rangle_B} \left| \int p^k (\sigma_A(\boldsymbol{p}) - \sigma_B(\boldsymbol{p})) d\boldsymbol{p} \right| \tag{5}$$

which is equivalent to

$$\%E_k = 100 \cdot \frac{4\pi N}{\langle p^k \rangle_B} \left| \int_0^\infty p^{k+2} (\sigma_A^0(p) - \sigma_B^0(p)) dp \right| \tag{6}$$

where the momentum shape function[14] $\sigma(\boldsymbol{p}) = \Pi(\boldsymbol{p})/N$ and its spherical average $\sigma^0(p)$ have been introduced. Based on the quality of the moments of momenta, the previous work by Hart and Thakkar found that DFT generally performs worse than HF.[8]

The integrands in eqs 5 and 6 are not strictly positive, and, hence, $\%E_k$ can still be zero when $\sigma_A(\boldsymbol{p}) \neq \sigma_B(\boldsymbol{p})$ if the positive and negative regions in the integrand cancel. There may be a high apparent similarity in a certain moment even when the overall electron momentum distributions differ significantly. Clearly, deviations in moments of momentum do not provide all information about the resemblance in shape between different methods.

In this work we mainly use the full $\Pi(\boldsymbol{p})$-distribution as source of information to compare momentum densities of different origins but in a similar way as for the study of the similarity between molecules.[7a] Intensive use will be made of the Euclidean distance between momentum shape functions[15] obtained using methods A and B:

$$D_{AB}(k) = \sqrt{\int (p^k \sigma_A(\boldsymbol{p}) - p^k \sigma_B(\boldsymbol{p}))^2 d\boldsymbol{p}} \tag{7}$$

Contrary to $\%E_k$ the integrand is always positive, so cancellation of error is impossible. For Gaussian type orbitals one finds that $D_{AB}(k)$ is subject to a lower limit $k \geq -1$. In the field of quantum similarity, eq 7 is commonly written as[7a]

$$D_{AB}(k) = \sqrt{I_{AA}(k) + I_{BB}(k) - 2I_{AB}(k)} \tag{8}$$

where $I_{AB}(k)$ represents the momentum space Quantum Similarity Measure or generalized overlap:[7a]

$$I_{AB}(k) = \int p^{2k} \sigma_A(\boldsymbol{p}) \sigma_B(\boldsymbol{p}) d\boldsymbol{p} \tag{9}$$

The factor p^{2k} in eq 9 is comparable to the factor p^k for the moments of momentum (eq 4) and highlights different **p**-space regions. The above-mentioned possibility of cancellation of error in $\%E_k$ can be investigated through comparison of $D_{AB}(k)$ with $\%E_k$ for values of k permitting evaluation of both quantities. As spherical averaged densities are quite often used, an obvious extension can be made to differences in spherically averaged electron momentum densities as

$$D_{AB}^0(k) = \sqrt{I_{AA}^0(k) + I_{BB}^0(k) - 2I_{AB}^0(k)} \tag{10}$$

$$I_{AB}^0(k) = \int_0^\infty p^{2k} \sigma_A^0(p) \sigma_B^0(p) dp \tag{11}$$

Here, the lower limit is given by $k \geq 0$. Note that a comparison with $\%E_k$ can be made either with $D_{AB}(k)$ or with $D_{AB}^0(k+2)$. For $k = -2$, however, $D_{AB}(k)$ does not exist (see above), and, hence, only $D_{AB}^0(0)$ can be used to interpret $\%E_{-2}$.

Of interest in the present study is how DFT performs in momentum space and particularly with respect to Hartree−

dx.doi.org/10.1021/ct400266g | J. Chem. Theory Comput. XXXX, XXX, XXX−XXX

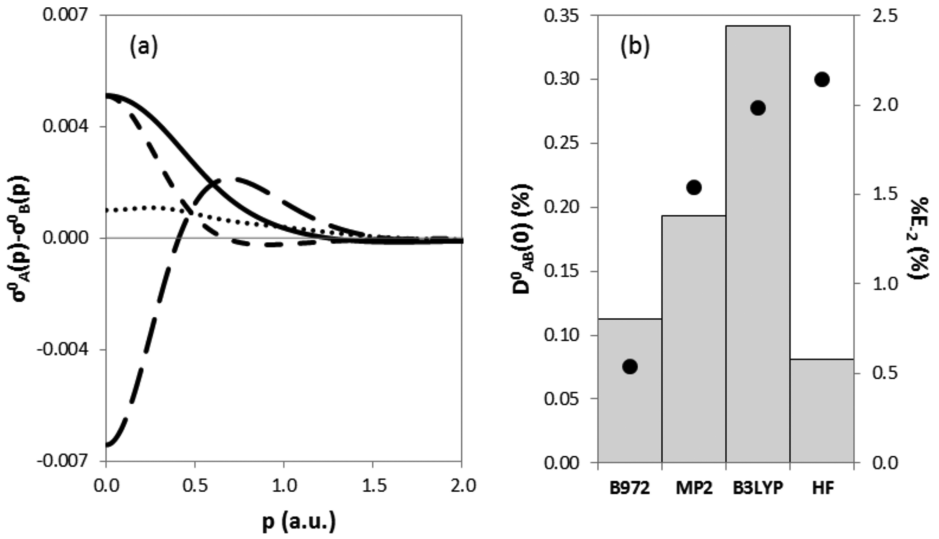

Figure 1. a. (left) The $(\sigma_A^0(p) - \sigma_B^0(p))$-distribution for N_2 with respect to B=CCSD and A being MP2 (short dashes), B972 (dots), B3LYP (full line), and HF (long dashes). **b.** (right) The corresponding $D_{AB}^0(0)$ (black dots) and $\%E_{-2}$ (columns).

Fock (HF). The interest in DFT derives from the fact that it makes quantum chemical calculations, including electron correlation, on large systems computationally feasible within an acceptable time frame. This is particularly convenient regarding the calculation of directional Compton profiles for solid-state systems. A recent study by Pisani and co-workers,[5] however, showed that the experimental directional Compton Profile of α-quartz is better reproduced by HF than by the DFT methods tested: B3LYP, PBEPBE, and LDA. Given the potential of DFT for computing data in the solid state, a better understanding of the performance of DFT methods in momentum space is desirable.

In addition to the mentioned experimental comparison,[5] other **p**-space studies also suggest that DFT does not reliably predict momentum space properties. From these studies,[8,9] it appears that approximate exchange-correlation functionals are largely optimized for position densities, and, as a result, it is not guaranteed that they reproduce the electron momentum distribution well. This was also the conclusion made by Ragot,[11e] who stated that approximate DFT *can* be - but not necessarily is - better than HF with respect to **p**-space properties. This raises the question whether there are DFT functionals currently available that allow improvement over HF since the previous studies only considered part of the wealth in approximate density functionals. Using the calculations described below, we examine the performance of such a large set of functionals.

COMPUTATIONAL DETAILS

To examine the performance of DFT in momentum space, we use an extensive set of small molecules and a wide set of theoretical methods and compute the moments of momentum and generalized overlap measures described above. The generalized overlap and the moments of momentum were calculated using home-developed programs. The moments of momentum were obtained analytically from the spherically averaged electron momentum density using confluent hypergeometric functions.[16] As validation of the routines, we find that the numerical implementation and analytical implementation differ insignificantly (equality up to at least 7 digits) and moreover that reproduced data coincide within numerical precision with those of Hart and Thakkar.[8] Using an extended strategy, we implemented a routine to calculate $I_{AB}(k)$ analytically as well. In contrast to the moments of momentum, $I_{AB}(k)$ contain 4-center integrals. Note that the integrals have to be evaluated for every power k in eq 9 separately. For the present study, where a large set of computational methods and molecules is used, the analytical routine was not considered cost-effective. We therefore opted to obtain the $I_{AB}(k)$ numerically using Gauss-Laguerre quadrature for the radial part of the integration and a Lebedev grid for the angular part. The different powers k are then easily implemented without a significant additional computational cost. The order of the Laguerre polynomials was 500, and the Lebedev grid contained 2030 points. Comparison with our analytical program indicated that under these circumstances the numerical integration for $I_{AB}(k)$ was correct up to at least 7 significant digits for $-1 \le k \le 2$.

For sake of having compatible results with the earlier study by Hart and Thakkar,[8] we used the same test set of 68 molecules with the all-electron MP2/6-311G* geometries taken from the NIST-database.[17] The choice of the set of functionals was made in order to contain many of the most popular ones[18] and to represent different types: L(S)DA, pure, Generalized Gradient Approximation (GGA), hybrid, double hybrid, long-range corrected, dispersion corrected, etc. A complete list of these functionals with appropriate literature references can be found in the Supporting Information. Single point calculations were performed using Gaussian-09.[19] The Dunning augmented correlation consistent aug-cc-pVTZ basis set was used throughout.[20]

Wiberg and co-workers[21] have shown that QCISD density matrices obtained using either the Slater determinant expansion or the Z-vector method are very similar. QCISD, however, can be regarded as an approximation of the CCSD method,[22] hence we opted to use CCSD Z-vector based density matrices, allowing a better comparison also to the results by Hart and Thakkar, who also used CCSD reference densities.[8]

Note that the DFT based $\Pi(\boldsymbol{p})$-distributions rely on the Fourier transformation of the position space density matrix since no universal density functional in **p**-space exists.[23] This entails the use of the Kohn−Sham Slater determinant which rather corresponds to a system of noninteracting electrons,

dx.doi.org/10.1021/ct400266g | J. Chem. Theory Comput. XXXX, XXX, XXX−XXX

albeit giving, in principle, the exact charge density. Even if the exact functional were known, there is no direct route to transform an electron density from **r** to **p** space, hence the need to return to the level of the density matrix.

RESULTS AND DISCUSSION

As an illustration of the results obtained, we first report **p**-space Euclidean distances $D^0_{AB}(0)$ for the N_2-molecule calculated using different computational methods. The $(\sigma^0_A(p) - \sigma^0_B(p))$-distribution with respect to B=CCSD for A=MP2, B972, B3LYP, and HF is plotted in Figure 1a. The integral of these distributions corresponds to $\%E_{-2}$ and is shown in Figure 1b together with $D^0_{AB}(0)$-values. We notice that for A=HF the $(\sigma^0_A(p) - \sigma^0_B(p))$-distribution shows the largest difference of all methods. However, as for HF this difference occurs with both signs over large areas, significant cancellation of error occurs leading to an artificially low value for $\%E_{-2}$. The Euclidean distance, through the square in the integrand, better reflects the rather poor $\sigma^0_A(p)$ as is shown in Figure 1b. Figure 1 clearly shows how it may be deceptive to conclude that DFT performs significantly worse than HF with respect to CCSD for $\Pi(\boldsymbol{p})$, and one must carefully distinguish between performance in generating a good quality $\Pi(\boldsymbol{p})$ and reproducing momentum moments.

Turning to the larger set of molecules, due to the large amount of data, we discuss only the performance for a few values of k and limit the presentation of numerical data to the union of the 15 best performing methods for each value of k discussed (best performing = lowest Euclidean distance with respect to CCSD). Table 1 shows the results for $D^0_{AB}(0)$ and $D_{AB}(k)$ with $k = -1, 0, 1, 2$ for this union (MP2, B972, M06, ωB97XD, τ-HCTH, mPW1PW91, TPSSh, B3PW91, mPW1PBE, B1B95, B3P86, HSE2PBE, BHandHLYP, τ-HCTHhyb, HCTH93, B2PLYP, B98, mPW2PLYP, BMK, LC-XαVWN, HF, ωB97X, LC-BVWN, LC-TPSSTPSS, O3LYP, LC-ωPBE). A color code is applied ranging from green for low values (high similarity) to red for high values (low similarity) in each column separately and allows to compare how well a method performs for either spherically averaged or nonaveraged $\sigma(\boldsymbol{p})$-distributions and in low or high momentum regions. All values correspond to averages over all molecules, hence the shape function is used to avoid bias introduced by the different number of electrons in the distances. LC denotes the inclusion of the long-range correction introduced by Iikura et al.[24] In order to evaluate the effect of LC on the performance of a method, the noncorrected functionals (BVWN, TPSSTPSS, and XαVWN) were added for comparison. For the performance of the other functionals, the reader is referred to the Supporting Information.

Starting with the average Euclidean distances for $D^0_{AB}(0)$ which measure the similarity in $\sigma^0(p)$ with respect to the reference, the color code in Table 1 reveals that different functionals can perform very differently (note again that many perform still worse but are only shown in the Supporting Information). As outlined in the Methodology section and illustrated in Figure 1b, $D^0_{AB}(0)$ is conceptually related to $\%E_{-2}$. The underlying $\langle p^{-2}\rangle$ has no straightforward physical meaning, although it has been proposed that half of its reciprocal value resembles a pseudokinetic energy.[25] Figure 2 depicts the average $D^0_{AB}(0)$ along with the average $\%E_{-2}$ and shows that there generally is a good correlation between both. As illustrated for N_2 above, the methods for which $\%E_{-2}$ does not follow the trend of the mean Euclidean distance reproduce the second negative moment artificially well due to a cancellation of errors. This occurs among others for M06, B972, HF, and τ-HCTH. On average, B972, M06, and HF reproduce $\langle p^{-2}\rangle$ even better than MP2. The standard deviations for the error on this moment of momentum, on the other hand, are 0.597, 0.583, 0.839, and 0.287%, respectively (see the Supporting Information for data on standard deviations). The inadequacy of MP2 at reproducing $\langle p^{-2}\rangle$ was reported by Hart and Thakkar as well.[8] Our results show that the underlying momentum distribution, however, is nonetheless better reproduced by MP2 compared to all other computational methods. We may conclude that the $\sigma^0(p)$-distributions calculated using the M06 and B972 functionals have near MP2-quality, yet the standard deviation on $D^0_{AB}(0)$ for these functionals is much larger (>0.2%) compared to MP2 (0.06%), hence making them less reliable in general. The LC does not improve the agreement with the $\sigma^0(p)$-distribution calculated at CCSD, which can be seen by the larger mean $D^0_{AB}(0)$ and $\%E_{-2}$ values for BVWN, TPSSTPSS, and XαVWN upon including LC. Based on the bar fillings in Figure 2 one can see that the $\sigma^0(p)$ distributions derived from hybrid functionals are generally superior to those from GGA's.

Based on 2 atoms and 8 molecules and a limited set of GGA functionals, Miguel and de la Vega[9] concluded that the BVWN radial momentum distributions $p^2\sigma^0(p)$ are the best over all GGA's considered by them but are still inferior to HF.

Table 1. Mean Euclidean Distances for the Selection of Computational Methods (See Text)[a]

Method	$D^0_{AB}(0)$	$D_{AB}(-1)$	$D_{AB}(0)$	$D_{AB}(1)$	$D_{AB}(2)$
MP2	0.1047	0.3815	0.1403	0.1066	0.1500
B972	0.1077	0.4018	0.1783	0.1944	0.3493
M06	0.1051	0.3977	0.1844	0.2151	0.3885
ωB97XD	0.1419	0.5110	0.1944	0.1925	0.3429
τ-HCTH	0.1409	0.5311	0.1998	0.2126	0.3929
mPW1PW91	0.1372	0.5015	0.2067	0.2052	0.3578
TPSSh	0.1258	0.4675	0.2069	0.2195	0.3911
B3PW91	0.1293	0.4741	0.2084	0.2143	0.3733
mPW1PBE	0.1389	0.5077	0.2093	0.2076	0.3612
B1B95	0.1406	0.5114	0.2102	0.2058	0.3563
B3P86	0.1152	0.4239	0.2112	0.2225	0.3812
HSE2PBE	0.1227	0.4500	0.2123	0.2137	0.3641
BHandHLYP	0.1247	0.4567	0.2155	0.1958	0.3115
τ-HCTHhyb	0.1509	0.5505	0.2220	0.2150	0.3738
HCTH93	0.1906	0.7038	0.2320	0.2168	0.3891
B2PLYP	0.1799	0.6546	0.2337	0.1770	0.2678
B98	0.1599	0.5805	0.2358	0.2143	0.3579
TPSSTPSS	0.1681	0.6189	0.2420	0.2358	0.4166
mPW2PLYP	0.1904	0.6919	0.2433	0.1776	0.2639
BMK	0.1321	0.4414	0.2445	0.2535	0.3533
BVWN	0.1836	0.6696	0.2449	0.2323	0.4212
LC-XαVWN	0.2190	0.7875	0.2489	0.1995	0.3705
XαVWN	0.1858	0.6789	0.2572	0.2531	0.4680
HF	0.1335	0.5037	0.2587	0.2534	0.4059
ωB97X	0.2042	0.7281	0.2596	0.2117	0.3470
LC-BVWN	0.2343	0.8374	0.2782	0.2133	0.3533
LC-TPSSTPSS	0.2305	0.8233	0.2850	0.2237	0.3600
O3LYP	0.2502	0.9075	0.2868	0.2202	0.3633
LC-ωPBE	0.2651	0.9461	0.2898	0.2087	0.3430

[a]A color code labels the performance of each method within each column separately.

dx.doi.org/10.1021/ct400266g | J. Chem. Theory Comput. XXXX, XXX, XXX−XXX

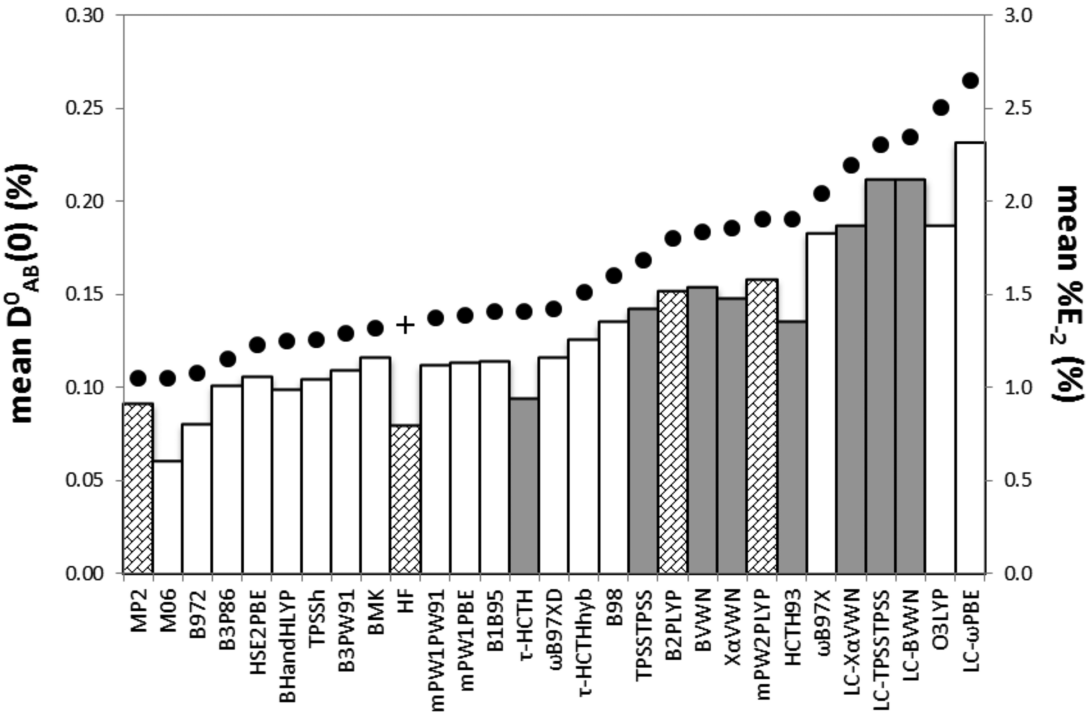

Figure 2. Mean $D^0_{AB}(0)$ and $\%E_{-2}$. The dots correspond to $D^0_{AB}(0)$ (HF is marked with a cross), the bars represent $\%E_{-2}$. The bar filling reflects the kind of method: hybrids (white), GGA's (gray), and other methods (MP2, HF, the double hybrid methods) are hatched.

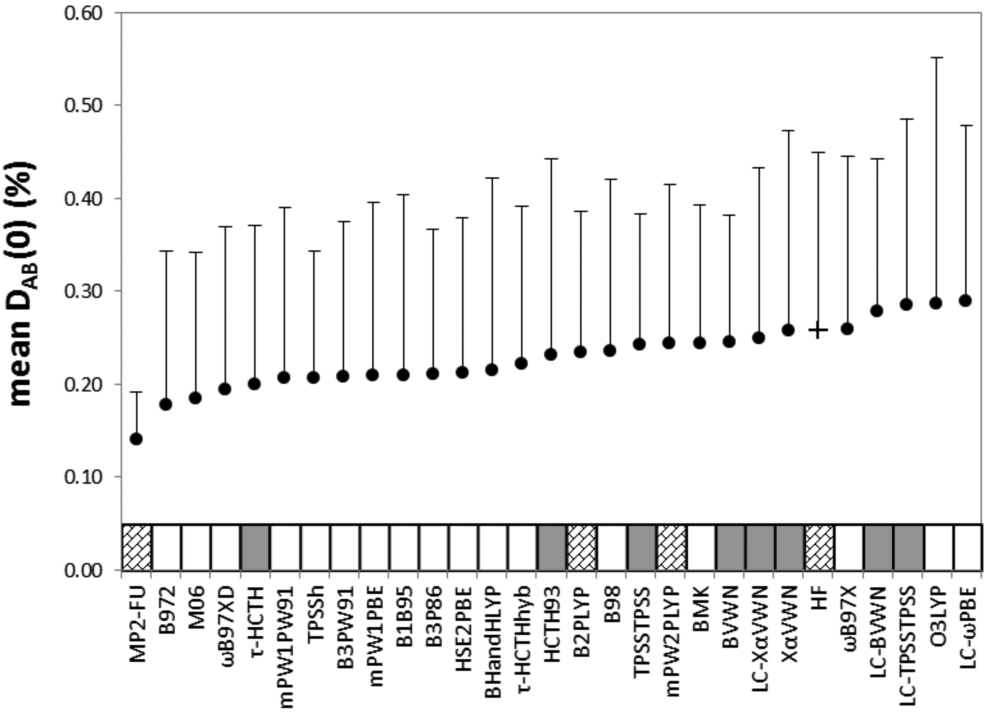

Figure 3. The average $D_{AB}(0)$ (black dots) and standard deviation (error bars) over all molecules with CCSD as reference. HF is marked with a cross. The bars on the bottom merely serve as an aid to distinguish the nature of the method (see Figure 2).

Inspection of our $\sigma^0(p)$-similarity data confirms BVWN to be the best among their set of GGA's.

Since the quality of the agreement of the $p^{-1}\sigma(\boldsymbol{p})$-distributions is very similar to the one found for $\sigma^0(p)$ (see Table 1), it will be discussed only briefly. Just as was the case for the $\sigma^0(p)$-distributions, the four best methods are MP2, M06, B972, and B3P86, and the LC-functionals are again worse at reproducing the $p^{-1}\sigma(\boldsymbol{p})$-distribution compared to their noncorrected counterparts. The mean distances $D_{AB}(-1)$ found for these distributions provide insight in $\%E_{-1}$. The first negative moment equals twice the value of the isotropic Compton Profile at zero momentum.[2] Consistent with the mean absolute percentage error on $\langle p^{-2}\rangle$ above, the error on $\langle p^{-1}\rangle$ is also artificially low for M06, B972, HF, and τ-HCTH.

dx.doi.org/10.1021/ct400266g | J. Chem. Theory Comput. XXXX, XXX, XXX−XXX

The cancellation of errors, however, is not as large as was the case for $\langle p^{-2}\rangle$, and, hence, MP2 is found most adequate to evaluate $\langle p^{-1}\rangle$ within the considered selection of methods.

Let us now address the mean Euclidian distances $D_{AB}(0)$ for the $\sigma(\boldsymbol{p})$ distribution, which reflect how well the normalized electron momentum distribution (without highlighting momentum regions) is approximated. As before, $D_{AB}(0)$ is conceptually related to $\%E_0$ which is zero because $\langle p^0\rangle$ equals the number of electrons for each molecule and for all methods. The obtained results are shown in Figure 3, where the standard deviations for $D_{AB}(0)$ are represented by error bars for each method. Clearly, MP2 − for which the mean $D_{AB}(0)$-value and the corresponding standard deviation is minimal − yields $\sigma(\boldsymbol{p})$ distributions most similar to CCSD. HF and the DFT methods, on the other hand, exhibit a much larger standard deviation making them less reliable. It is important to note that quite a few hybrid and GGA functionals perform better than HF. The majority of hybrid functionals is more accurate than GGA functionals at reproducing $\sigma(\boldsymbol{p})$, with the exception of τ-HCTH which performs significantly better than the other GGA's. The double hybrid methods mPW2PLYP and B2PLYP do not particularly improve over other DFT-methodologies. The three optimal functionals for $\sigma(\boldsymbol{p})$ calculations are B972, M06, and ωB97XD. It is worth noting that ωB97X performs worse than ωB97XD. The inclusion of atom−atom dispersion corrections clearly improves the agreement with the CCSD calculations. Moreover, this observation holds for the other values of k as well (see Table 1). Figure 3 shows that the LC long-range correction has a rather unpredictable effect. While the XαVWN momentum distributions show some improvement upon including it, the BVWN and TPSSTPSS functionals exhibit opposite behavior.

The results for the BLYP, B1LYP, B3LYP, PBEPBE, PBE1PBE, and LSDA functionals, previously studied by Hart and Thakkar,[8] are not included here due to not belonging to the top-15 for any value of k or $D^0_{AB}(0)$ but are available in the Supporting Information. Apart from PBE1PBE, our results support their conclusions that these functionals are inferior to HF for all Euclidean distances considered here. These findings are also in line with the observations made by Pisani and coworkers,[5] who found that the experimental directional Compton Profile matches better with the HF calculation than with those obtained using either B3LYP or PBEPBE. Note, however, that there is no direct relation between the quality of $\sigma(\boldsymbol{p})$ of a method with respect to a high level reference and the agreement in directional Compton profiles. Even though a high quality $\sigma(\boldsymbol{p})$-distribution naturally gives rise to a high quality directional Compton profile, a poorer $\sigma(\boldsymbol{p})$ may also lead to good agreement for the directional Compton Profile when mismatching regions cancel upon cylindrical averaging. The latter may be detected, however, by inspecting Compton profile anisotropies rather than the directional Compton profiles themselves.

Compared to the $\sigma^0(p)$-distributions (Figure 2), we see that far more functionals outperform HF at generating the full $\sigma(\boldsymbol{p})$-counterparts. This observation is rooted in the fact that for an individual molecule spherical averaging may either enhance or deteriorate the similarity with respect to the reference and the degree to which depends on the computational method considered. Considering a large set of molecules, however, we found that the mean $D^0_{AB}(0)$ is smaller than the mean $D_{AB}(0)$ for each method and, thus, that due to the loss of anisotropy, the similarity is usually enhanced with respect to the CCSD reference. The fact that the average degree of similarity enhancement depends on the method under consideration has important implications. As outlined above, for example, the $\sigma(\boldsymbol{p})$-distribution is not reproduced particularly well by HF. On average, however, its spherical average $\sigma^0(p)$ is relatively good. This is illustrated in Figure 4, where the mean distances for the

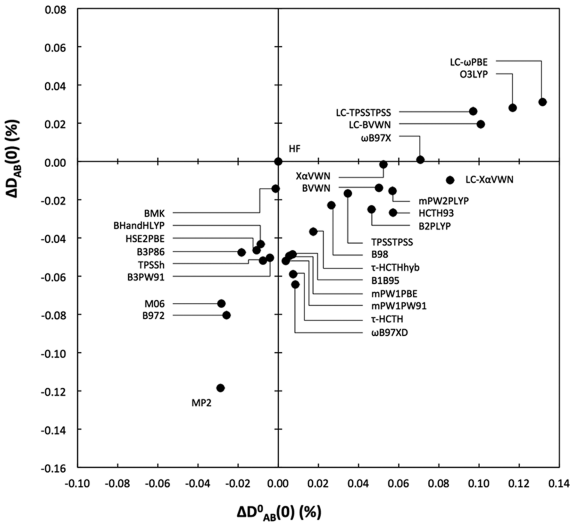

Figure 4. The average Euclidean distance $D_{AB}(0)$ of the momentum shape function with respect to the CCSD reference versus the average distance $D^0_{AB}(0)$ for their spherically averaged counterparts. The data points are plotted relative to HF.

$\sigma(\boldsymbol{p})$ and $\sigma^0(p)$ distributions are plotted against one another with respect to HF for the selection of computational methods. Whereas the average similarity enhancement is smallest for MP2, the effect is very large in the case of HF (the upper left quadrant in Figure 4 is empty). These results imply that electron correlation effects present in $\sigma(\boldsymbol{p})$ are largely wiped out upon spherical averaging. The latter is consistent with the earlier findings of Kulkarni and Gadre[11a] who reported that correlated $\sigma(\boldsymbol{p})$-distributions merely have higher curvatures and hence greater falloff and increase of electronic momenta compared to HF distributions. Furthermore, Crittenden and Bernard[26] also reported that electron correlation effects on $\sigma^0(p)$ are fairly faint and maximally induce relative errors of 0.5%. We may hence conclude that improvement over HF with respect to isotropic Compton profiles is difficult. Whether this holds true for directional Compton profiles as well is a different matter, yet it is possible that cylindrical averaging of $\sigma(\boldsymbol{p})$ has a similar effect.

As can be seen in Figure 4, the lower left quadrant contains only 8 DFT functionals that on average outperform HF in **p**-space, both at reproducing $\sigma(\boldsymbol{p})$ as well as $\sigma^0(p)$. The lower right quadrant contains computational methods that reproduce $\sigma(\boldsymbol{p})$ better than HF, but spherical averaging does not enhance the similarity with the CCSD $\sigma^0(p)$-distribution as much as for HF. The upper right quadrant contains functionals that (on average) are inferior to HF, and one may hence argue whether Coulomb correlation is adequately introduced by them in **p**-space. In addition to Figure 4, many popular DFT methods like B3LYP, CAM-B3LYP, M06-L, and BHandH belong to this region (Supporting Information). We stress that the present study emphasizes only on the quality of the $\sigma(\boldsymbol{p})$ and $\sigma^0(p)$ distributions and for example cannot predict the agreement

dx.doi.org/10.1021/ct400266g | J. Chem. Theory Comput. XXXX, XXX, XXX−XXX

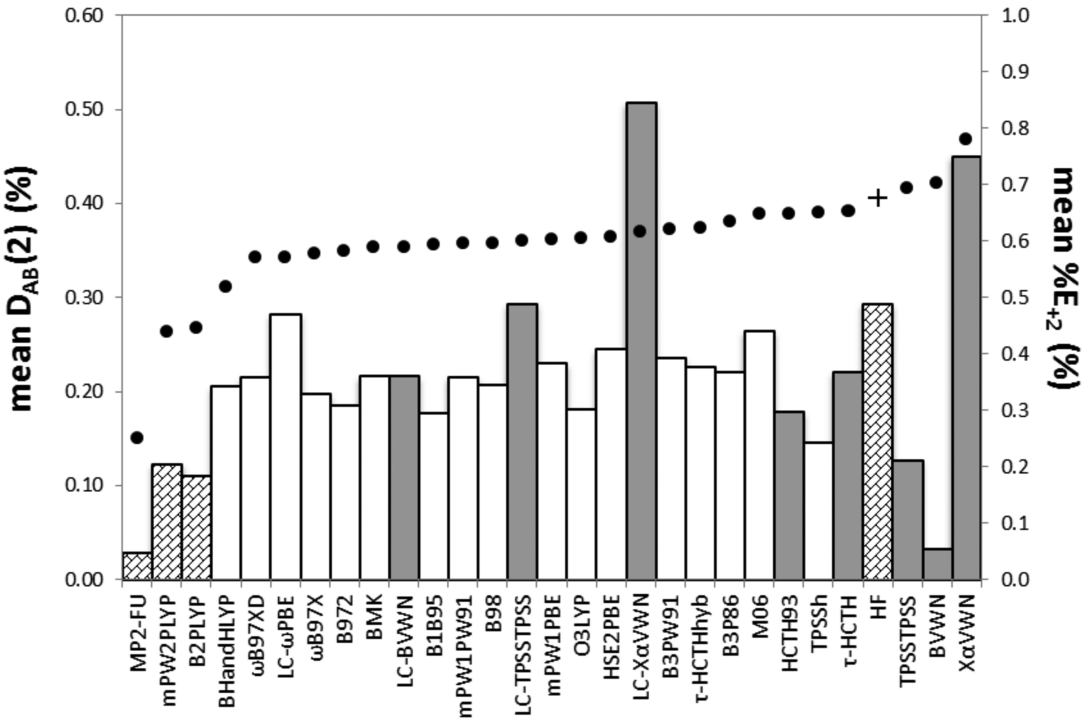

Figure 5. Mean $D_{AB}(2)$ and $\%E_{+2}$. The dots corresponds to the mean $D_{AB}(2)$ (HF is marked with a cross), the bars represent $\%E_{+2}$. The bar filling serves as an aid to distinguish the nature of the method (see Figure 2).

between Dyson orbitals and Kohn−Sham orbitals which are employed in electron momentum spectroscopy.

When higher momentum regions are emphasized - as in the $p.\sigma(\boldsymbol{p})$ and $p^2.\sigma(\boldsymbol{p})$ distributions - a rather different picture is found. In these regions of the electron momentum distribution, MP2 and the double hybrid methods are clearly superior. Many DFT methodologies improve over HF in these **p**-space regions, yet they have more or less the same agreement with respect to the reference. Contrary to the low momentum region, the inclusion of LC improves the $p.\sigma(\boldsymbol{p})$ and $p^2.\sigma(\boldsymbol{p})$ distributions. This behavior is unexpected considering the fact that the **r**- and **p**-spaces are reciprocal: what is far from the nuclei in position space converts to close to the origin in momentum space. As a consequence, an improvement of the valence region of $\rho(\boldsymbol{r})$ should coincide with a better description of the low momentum region of $\sigma(\boldsymbol{p})$. In case of LC, the opposite is observed: we obtain an improvement of the higher momentum regions at cost of the density at low momenta.

The mean values for $D_{AB}(1)$ and $D_{AB}(2)$ reflect how well the integrands of the $\langle p^{+1}\rangle$ and $\langle p^{+2}\rangle$ moments (eq 5) resemble the CCSD reference. While the first positive moment of momentum $\langle p^{+1}\rangle$ corresponds to the expectation value of momentum magnitude, the second positive moment of momentum equals twice the kinetic energy of the molecular system.[2] Figure 5 illustrates that many functionals have $p^2.\sigma(\boldsymbol{p})$ distributions that on average are equally close to the reference, yet they differ significantly in shape and hence lead to a large variety of $\%E_{+2}$ values. Note how BVWN reproduces $\langle p^{+2}\rangle$ almost as accurate as MP2 ($\%E_{+2}$ is 0.054 and 0.048%, respectively). BVWN even has a lower standard deviation for $\%E_{+2}$: 0.027 versus 0.144%. This is a consequence of a strikingly consistent cancellation of errors within the integral of eq 5 and must be inherent to the BVWN functional over all molecules in our test set. This feature is delicate, however, as can be seen by comparison with LC-BVWN. The inclusion of LC ameliorates the $p^2.\sigma(\boldsymbol{p})$ distribution leading to a lower value for $D_{AB}(2)$ yet coincides with a significantly higher error for the second positive moment. This phenomenon occurs for the TPSSTPSS and XαVWN functionals when LC is included as well.

Summarizing, the performance of density functionals, via a Kohn−Sham density matrix, in momentum space depends significantly on the value k for both the moments of momentum and the computed Euclidean distances. From this work, it is found that also the differences in moments of momentum may significantly differ from the agreement in k-weighted density functions in **p**-space. This is due to the possible cancellation of error in computing $\%E_k$ values which cannot occur in Euclidean distances.

In line with Ragot,[11e] approximate DFT can outperform HF in momentum space even without the inclusion of self-interaction corrections; however, much depends on the functional used. Concerning the results of Pisani et al.,[5] showing that HF corresponds better with experimental directional Compton profiles than DFT, our results suggest testing of the presently best performing functionals. One should be aware that the cylindrical averaging, which is necessary to calculate directional Compton profiles, may lead to similarity enhancement as well and may be more significant for some methods than for others.

CONCLUSION

The performance of several computational methods in **p**-space with respect to CCSD was investigated. Our results show that the absolute percentage errors on the moments of momentum are not fully adequate for comparing the accuracy of computational methods since they are prone to cancellation of errors. The Euclidean distance between momentum distributions highlighting different regions of the electron momentum density with respect to a reference, on the other

dx.doi.org/10.1021/ct400266g | J. Chem. Theory Comput. XXXX, XXX, XXX−XXX

hand, represents an unbiased measure for the reliability of a computational method.

Our study shows that MP2 resembles the CCSD reference distributions better than any DFT methodology for both low and high momentum regions. Only 8 DFT functionals outperform HF on average both at approximating the momentum shape function as well as its spherically averaged counterpart. These functionals are M06, B972, B3P86, HSE2PBE, BHandHLYP, TPSSh, B3PW91, and BMK. This implies that for HF the similarity with respect to the CCSD reference is considerably enhanced upon spherical averaging, indicating that electron correlation effects are wiped out substantially due to this procedure.

With respect to the development of DFT functionals and their application in momentum space, care should be taken with long-range corrections. Our results show that within the set of molecules considered, it improves the medium and high momentum region at cost of the chemically important density at low momentum. This is intriguing, because an improvement of the charge density at large distances is expected to correspond with an improvement of the low momentum region of the electron momentum density.

■ ASSOCIATED CONTENT

Supporting Information

A list of the molecules employed in the present study. A list of the studied functionals with their literature references. Numerical data on average Euclidean distances $D^0_{AB}(0)$ and $D_{AB}(k)$ with $k = -1, 0, 1, 2$, including their standard deviation. The $\%E_k$ values with k ranging from -2 to 4 together with the corresponding standard deviation for each studied method. More extensive figures for Euclidean distances and $\%E_k$ covering all studied functionals. This material is available free of charge via the Internet at http://pubs.acs.org.

■ AUTHOR INFORMATION

Corresponding Author

*E-mail: patrick.bultinck@ugent.be.

Notes

The authors declare no competing financial interest.

■ ACKNOWLEDGMENTS

The computational resources (STEVIN Supercomputer Infrastructure) and services used in this work were kindly provided by Ghent University, the Flemish Supercomputer Center (VSC), the Hercules Foundation, and the Flemish Government−department EWI. We wish to thank Dr. Michael Deleuze for his comments. We gratefully acknowledge FWO-Flanders and the research council of Ghent University for financial support.

■ REFERENCES

(1) Dirac, P. A. M. The physical interpretation of the quantum dynamics. *Proc. R. Soc. London, Ser. A* **1927**, *113*, 621−641.

(2) Thakkar, A. J. The momentum density perspective of the electronic structure of atoms and molecules. *Adv. Chem. Phys.* **2004**, *128*, 303−352.

(3) Defranceschi, M.; Delhalle, J.; Windt, L.; Fischer, P.; Fripiat, J.; Ellinger, Y. Quantum Chemistry Computations in Momentum Space. In *Strategies and Applications in Quantum Chemistry*, 1st ed.; Ellinger, Y., Defranceschi, M., Eds.; Springer: Netherlands: 2002; Vol. *14*, pp 139−158.

(4) Kaijser, P.; Smith Jr., V. H. On inversion Symmetry in Momentum Space. In *Quantum Science Methods and Structure. A tribute to Per Olov Löwdin*, 1st ed.; Calais, J. L., Goscinski, O., Linderberg, J., Öhrn, Y., Eds.; Plenum Press: New York, 1976; pp 417−425.

(5) Pisani, C.; Erba, A.; Casassa, S.; Itou, M.; Sakurai, Y. Anisotropy of the electron momentum distribution in alpha-quartz investigated by Compton scattering and ab initio simulations. *Phys. Rev. B: Condens. Matter Mater. Phys.* **2011**, *84*, 1−12.

(6) Cooper, M. J. Compton-scattering and electron momentum determination. *Rep. Prog. Phys.* **1985**, *48*, 415−481.

(7) (a) Allan, N. L.; Cooper, D. L. Momentum-Space Electron-Densities and Quantum Molecular Similarity. In *Molecular Similarity I*, 1st ed.; Sen, K., Ed.; Springer: Berlin, Heidelberg: 1995; Vol. *173*, pp 85−111. (b) Measures, P. T.; Mort, K. A.; Allan, N. L.; Cooper, D. L. Applications of momentum-space similarity. *J. Comput.-Aided Mol. Des.* **1995**, *9*, 331−340. (c) Angulo, J. C.; Antolin, J. Atomic quantum similarity indices in position and momentum spaces. *J. Chem. Phys.* **2007**, *126*, 1−5. (d) Vivas-Reyes, R.; Arias, A.; Vandenbussche, J.; Van Alsenoy, C.; Bultinck, P. Quantum similarity of isosteres coordinate versus momentum space and influence of alignment. *J. Mol. Struct. Theochem.* **2010**, *943*, 183−188.

(8) Hart, J. R.; Thakkar, A. J. Moments of the electron momentum density: requirements for ab initio and density functional theory calculations. *Int. J. Quantum Chem.* **2005**, *102*, 673−683.

(9) Miguel, B.; de la Vega, J. M. G. Influence of electronic correlation in monoelectronic density in p-space. *Theor. Chem. Acc.* **2007**, *118*, 723−732.

(10) Bultinck, P.; Girones, X.; Carbo-Dorca, R. Molecular quantum similarity: Theory and applications. In *Rev. Comput. Chem.*, 1st ed.; Lipkowitz, K. B., Larter, R., Larter, T. R., Eds.; John Wiley & Sons, Inc.: Hoboken, NJ, USA, 2005; Vol. *21*, pp 127−207.

(11) (a) Kulkarni, S. A.; Gadre, S. R. How reliable are topographical characteristics of Hartree-Fock level molecular electron momentum densities? *Chem. Phys. Lett.* **1997**, *274*, 255−263. (b) Wang, J. H.; Clark, B. J.; Schmider, H.; Smith, V. H. Topological analysis of electron momentum densities and the bond directional principle: the first-row hydrides, AH, and homonuclear diatomic molecules, A2. *Can. J. Chem.* **1996**, *74*, 1187−1191. (c) Thakkar, A. J.; Sharma, B. S. Electron momentum densities near zero-momentum. *J. Mol. Struct. Theochem.* **2000**, *527*, 221−227. (d) Zope, R. R. Momentum-space properties of atoms: application of the generalized-gradient approximation. *Phys. Rev. A* **2000**, *62*, 1−4. (e) Ragot, S. Exact Kohn-Sham versus Hartree-Fock in momentum space: examples of two-fermion systems. *J. Chem. Phys.* **2006**, *125*, 1−10.

(12) *Compton scattering: the investigation of electron momentum distributions*; Williams, B. G., Ed.; McGraw-Hill International: New York, 1977.

(13) (a) Becker, P. J.; Gillet, J. M.; Cortona, P.; Ragot, S. Complementary aspects of charge and momentum density for the study of the chemical bond. *Theor. Chem. Acc.* **2001**, *105*, 284−291. (b) Pisani, C.; Itou, M.; Sakurai, Y.; Yamaki, R.; Ito, M.; Erba, A.; Maschio, L. Evidence of instantaneous electron correlation from Compton profiles of crystalline silicon. *Phys. Chem. Chem. Phys.* **2011**, *13*, 933−936.

(14) Parr, R. G.; Bartolotti, L. J. Some remarks on the density functional theory of few-electron systems. *J. Phys. Chem.* **1983**, *87*, 2810−2815.

(15) Carbo-Dorca, R. Scaled Euclidian distances: a general dissimilarity index with a suitably defined geometrical foundation. *J. Math. Chem.* **2012**, *50*, 734−740.

(16) Thakkar, A. J.; Sharma, B. S. A fresh look at the computation of spherically averaged electron momentum densities for wave functions built from Gaussian-type functions. *Int. J. Quantum Chem.* **2001**, *85*, 258−262.

(17) Johnson, R. D., III NIST Computational Chemistry Comparison and Benchmark Database, Number 101 Release 15b. http://cccbdb.nist.gov/ (accessed April 31, 2013).

(18) Popularity poll density functionals 2013. www.marcelswart.eu/dft-poll (accessed June 27, 2013).
(19) Frisch, M. J.; Trucks, G. W.; Schlegel, H. B.; Scuseria, G. E.; Robb, M. A.; Cheeseman, J. R.; Scalmani, G.; Barone, V.; Mennucci, B.; Petersson, G. A.; Nakatsuji, H.; Caricato, M.; Li, X.; Hratchian, H. P.; Izmaylov, A. F.; Bloino, J.; Zheng, G.; Sonnenberg, J. L.; Hada, M.; Ehara, M.; Toyota, K.; Fukuda, R.; Hasegawa, J.; Ishida, M.; Nakajima, T.; Honda, Y.; Kitao, O.; Nakai, H.; Vreven, T.; Montgomery, J. A., Jr.; Peralta, J. E.; Ogliaro, F.; Bearpark, M.; Heyd, J. J.; Brothers, E.; Kudin, K. N.; Staroverov, V. N.; Kobayashi, R.; Normand, J.; Raghavachari, K.; Rendell, A.; Burant, J. C.; Iyengar, S. S.; Tomasi, J.; Cossi, M.; Rega, N.; Millam, J. M.; Klene, M.; Knox, J. E.; Cross, J. B.; Bakken, V.; Adamo, C.; Jaramillo, J.; Gomperts, R.; Stratmann, R. E.; Yazyev, O.; Austin, A. J.; Cammi, R.; Pomelli, C.; Ochterski, J. W.; Martin, R. L.; Morokuma, K.; Zakrzewski, V. G.; Voth, G. A.; Salvador, P.; Dannenberg, J. J.; Dapprich, S.; Daniels, A. D.; Farkas, Ö.; Foresman, J. B.; Ortiz, J. V.; Cioslowski, J.; Fox, D. J. *Gaussian 09*, Revision A.2; Gaussian, Inc.: Wallingford, CT, 2009.
(20) Kendall, R. A.; Dunning, T. H.; Harrison, R. J. Electron-affinities of the 1st-row atoms revisited - systematic basis-sets and wave-functions. *J. Chem. Phys.* **1992**, *96*, 6796−6806.
(21) Wiberg, K. B.; Hadad, C. M.; LePage, T. J.; Breneman, C. M.; Frisch, M. J. Analysis of the effect of electron correlation on charge density distributions. *J. Chem. Phys.* **1992**, *96*, 671−679.
(22) (a) Scuseria, G. E.; Schaefer, H. F. Is coupled cluster singles and doubles (CCSD) more computationally intensive than quadratic configuration-interaction (QCISD). *J. Chem. Phys.* **1989**, *90*, 3700−3703. (b) Paldus, J.; Cizek, J.; Jeziorski, B. Coupled cluster approach or quadratic configuration-interaction. *J. Chem. Phys.* **1989**, *90*, 4356−4362.
(23) Henderson, G. A. Variational theorems for the single-particle probability density and density-matrix in momentum space. *Phys. Rev. A* **1981**, *23*, 19−20.
(24) Iikura, H.; Tsuneda, T.; Yanai, T.; Hirao, K. A long-range correction scheme for generalized-gradient-approximation exchange functionals. *J. Chem. Phys.* **2001**, *115*, 3540−3544.
(25) Cooper, D. L.; Ponec, R. Anatomy of bond formation: insights from the analysis of domain-averaged Fermi holes in momentum space. *Int. J. Quantum Chem.* **2009**, *109*, 2383−2392.
(26) Crittenden, D. L.; Bernard, Y. A. Compact expressions for spherically averaged position and momentum densities. *J. Chem. Phys.* **2009**, *131*, 1−7.